Astron. Astrophys. 341, 896–901 (1999)

ASTRONOMY AND ASTROPHYSICS

Velocity distribution function anisotropy of soft X-ray generated photoelectrons and resulting Hα polarization in solar flares

J.-C. Hénoux[1] **and M. Karlický**[2]

[1] Observatoire de Paris, DASOP-URA2080 (CNRS), F-92195 Meudon Cedex, France
[2] Astronomical Institute of the Academy of Sciences of Czech Republic, CZ-25165 Ondřejov, Czech Republic

Received 14 August 1998 / Accepted 27 October 1998

Abstract. Soft X-rays irradiation of the solar atmosphere during solar flares generates photoelectrons which have an anisotropic velocity distribution. Using a 1-D test particle code, the anisotropy of the photoelectrons velocity distribution is derived, and the maximum degree of linear polarization in the hydrogen Hα and Hβ lines that photoelectrons could generate by impact is estimated. Over a band pass of 0.75 and 0.5 Å, the net polarization degree expected in both lines is predicted not to exceed 0.2%. Therefore, soft X-ray irradiation cannot explain the one order of magnitude higher degree of linear polarization observed in solar flares.

Key words: line: formation – polarization – Sun: flares – Sun: particle emission – Sun: X-rays, gamma rays

1. Introduction

Chromospheric hydrogen Balmer lines Hα and Hβ have been found to be linearly polarized in solar flares. Hα polarization was observed in 2D filtergrams obtained with a monochromatic Lyot filter centered on the Hα line center with a 0.75 Å bandpass (Vogt and Hénoux, 1996). Independently, in other events (Firstova et al., 1997) the wavelength dependence of the linear polarization along the Hα and Hβ lines profiles was derived from spectroscopic observations.

In solar flare Hα filtergrams, the highest number of pixels emitting polarized Hα radiation is observed near the time of the maximum of soft X-ray emission. The degree of linear polarization reaches 5 to 10% and the direction of polarization in most of the flaring region is within 20 degree of the flare to disk center direction. In Hα flare spectra obtained after the flare impulsive phase, the dominant direction of polarization is also radial. In Hβ, the polarization is weaker and no net direction of polarization has been found yet.

The observed polarization indicates that energetic particles – electrons, protons or ions – with an energy high enough to collisionally excite the hydrogen Hα line are present in the solar chromosphere during solar flares with an anisotropic velocity distribution function. Such anisotropy may be associated with atmospheric bombardment by particle beams with a velocity distribution function symmetrical around the vertical direction and energies below 50 eV for electrons and 200 keV for protons. Since low energy electrons (E $\leq$ 50 eV) are strongly scattered in Coulomb collisions with local hydrogen atoms, low energy protons (E $\leq$ 200 keV) are the best candidates to explain the observed polarization, if due to vertically propagating particle beams.

However, photoionization by soft X-ray photons generates photoelectrons with a anisotropic velocity distribution function. Later, interactions with background thermal particles, electrons, ions and neutral hydrogen atoms, modify their velocity distribution function. Then, depending on the degree of anisotropy left and on the local density of photoelectrons relative to the thermal particles density, the collisional excitation of the Hα line can lead to linearly polarized line emission, and the aim of this paper is to estimate the order of magnitude of the resulting degree of linear polarization.

2. Main properties of impact polarization

2.1. Polarization generated by a monenergetic beam of particles

An anisotropy in the velocity distribution function of particles collisionally exciting an atom introduces a preferred direction and is reflected both by an anisotropy of the angular distribution of the intensity of the emitted radiation and by its linear polarization. This polarization results from the generated unequal population of the angular momentum substates (Percival and Seaton, 1959; Kleinpoppen, 1969; Heddle, 1979; Hénoux and Vogt, 1998). Calling respectively $I_{\parallel}$ and $I_{\perp}$ the intensities of the vibrations parallel and perpendicular to the plane defined by the beam and the line of sight and β the angle between the beam and the direction of observation, the polarization $P(\beta, E)$ is defined by

$$P(\beta, E) = (I_{\parallel} - I_{\perp})/(I_{\parallel} + I_{\perp}). \quad (1)$$

Simple geometrical considerations show that:

Send offprint requests to: J.C. Hénoux
Correspondence to: J.C. Hénoux

$$P(\beta, E) = P(90^\circ, E)\frac{\sin^2\beta}{1 - P(90^\circ, E)\cos^2\beta}, \quad (2)$$

where $P(90^\circ, E)$ is the maximum of polarization observable at 90° from the beam direction. $P(90^\circ, E)$ is a function of the nature of the particle – electron, proton, ion – and of the particle energy (Werner and Schartner, 1996). $P(\beta, E)$ changes of sign, from positive to negative, for a turn over energy E_0 that is of about 200 eV for electrons and 200 keV for protons.

2.2. Impact polarization generated by monoenergetic particles with a given velocity distribution $f(v, \alpha)$

Assuming axial symmetry around the beam direction of propagation, the degree of polarization $P(\theta, E)$, where θ is the angle between the line of sight and the symmetry axis, produced by particles of energy E, is defined by Eq. 1 where the intensities $I_\parallel$ and $I_\perp$ correspond respectively to vibrations parallel and perpendicular to the plane defined by the symmetry axis – usually the local solar vertical – and the line of sight and where β is replaced by θ. $P(\theta, E)$ can be related to the first even moments J_0 and J_2 of the particle velocity distribution function $f(v, \alpha)$ (Hénoux et al. 1983); these moments are defined by:

$$J_n = \int_0^\pi f(v, \alpha)\cos^n\alpha\,\sin\alpha\,d\alpha, \quad (3)$$

where α is the angle between the particle velocity vector and the beam axis of symmetry. The polarization is obtained by replacing in Eq. 2 $P(90^\circ, E)$ by $\mathcal{P}(90^\circ, E)$ with

$$\begin{aligned}\mathcal{P}(90^\circ, E) &= \frac{P(90^\circ, E)\,(3J_2 - J_0)}{2J_0 + P(90^\circ, E)(J_2 - J_0)} \\ &\simeq P(90^\circ, E)(\frac{3J_2}{2J_0} - 1). \end{aligned} \quad (4)$$

2.3. Impact polarization generated by no monoenergetic particles

In order to find the net polarization degree $P(\theta)$ produced by particles of various energies, integration must be made over the particle energy range. That leads to:

$$P(\theta) = \mathcal{P}(90^\circ)\frac{\sin^2\theta}{1 - \mathcal{P}(90^\circ)\cos^2\theta}, \quad (5)$$

with

$$\mathcal{P}(90^\circ) \simeq \frac{\int_{v_0}^\infty P(90^\circ, E)\,(3J_2 - J_0)v\sigma(v)dv}{\int_{v_0}^\infty 2J_0 v\sigma(v)dv}. \quad (6)$$

and

The angular distributions of photoelectrons of various energies required to estimate the polarization degree are derived below.

3. Anisotropy of the photoelectron velocity distribution function

3.1. Test particles model

In the present study, the evolution of the distribution function of photoelectrons, represented by test particles, under the influence of photoelectron-electron, photoelectron-proton and photoelectron-neutral hydrogen collisions, in a vertical and homogeneous magnetic field, is computed. Throughout the paper, except where expressed explicitly, c.g.s. units are used.

Photoelectrons are not emitted isotropically. In the energy range considered, the photoelectron number flux is proportional to $\sin^2\gamma$ (Evans, 1955), γ being the angle between the phoelectron traveling direction and the direction of photon propagation. For an irradiation along the local solar vertical, this maximum is in the horizontal direction. Since the magnetic field is vertical the pitch angle α is equal to γ.

Photoelectrons are represented by a large number of numerical electrons. In the present simulations, the relative total number of photoelectrons of energies 1 keV, 0.5 keV, and 0.25 keV, generated at specified heights were taken from previous studies of Hénoux and Nakagawa (1977) (noted as HN) that used the HSRA (Gingerich et al. 1971) quiet sun model (see also Hénoux and Rust, 1980). Following HN, their rate of generation is the highest at 675, 980 and 1380 km heights. These rates of photoelectron generation, and consequently the photoelectron energy flux can be changed by modifying the statistical weights of the numerical photoelectrons, which express the ratio between real and numerical photoelectron densities.

The energy losses and the change of pitch angle of photoelectrons, due to collisions with the background plasma electrons and neutral hydrogen atoms, were calculated according to formulas expressing the mean variation of the photoelectron energy and of the square of the deflection angle Θ after propagating over a distance L, as given in Emslie (1978) and Bai (1982):

$$\Delta E = -\frac{4\pi e^4}{m_e v^2}(n_e\Lambda + n_n\Lambda')L, \quad (7)$$

$$\langle\Theta^2\rangle = \frac{16\pi e^4}{3m_e^2 v^4}(3n_e\Lambda + n_n\Lambda'')L, \quad (8)$$

where e and m_e are the electron charge and mass, n_e and n_n are the electron and neutral hydrogen densities of the background plasma, v is the photoelectron velocity; Λ is the Coulomb logarithm and Λ' and Λ'' are effective Coulomb logarithms as defined in Brown (1973) and Emslie (1978).

The Monte Carlo method (Bai, 1982) was used to follow the evolution of the photoelectron distribution function. At every time step τ, the azimuthal deflection angle Φ_s was selected randomly over the interval 0 – 2π. Then, using the Eq. 8 that gives the rms deflection angle and assuming a Gaussian distribution of the deflection angle Θ_s, a new pitch angle Θ_2 after deflection was computed, such as

$$\cos\Theta_2 = \cos\Theta_1\cos\Theta_s + \sin\Theta_1\sin\Theta_s\cos\Phi_s. \quad (9)$$

Due to the strong effect of collisions, height changes are very small in comparison to chromospheric extension. Therefore, photoelectrons are scattered and stopped nearly at the position, where they are generated. Nevertheless, in this general model, the change of photoelectron positions was included in computing their velocity distribution functions. The motions of all the numerical photoelectrons in the atmosphere along the vertical magnetic field lines were computed. At every time step, positions of photoelectrons with a vertical component v_z of velocity in the solar atmosphere are changed as follows

$$h_{new} = h_{old} + v_z \Delta t, \tag{10}$$

where h_{new} and h_{old} are new and old heights of the photoelectron before and after an interaction with a local particle.

Since, in the case of strong collisions, phoelectrons remain at the place where they were generated, the mean characteristics of the angular dependence of the particles velocity distribution function was derived by integrating over time the energy and angular distribution of the injected particles, until their energy becomes close to the thermal energy of the medium.

At the beginning of the X-ray irradiation, photoelectrons are created and their number density increases in the atmosphere. At a saturation time t_S, a saturation level is reached such that the total number of photoelectrons generated over all the total energy range, per unit volume and per unit of time, is just equal to the number of photoelectrons that loose, per unit volume and per unit time, their non-thermal energy in collisions with the ambient particles and are thermalized. Then, at saturation the photoelectron density n_{ph}^S is just the number of previously deposited photoelectrons per unit volume that are left with a energy above the local thermal energy. Computations were made until this saturation state was reached.

Accordingly to HN, the ratios of the fluxes of the numerical photoelectrons injected in three energy bands (0.–0.333 keV; 0.333 keV – 0.666 keV; 0.666 keV–1 keV), assimilated to delta functions, were taken respectively as: a) at 675 km height, 27:40:7 numerical photoelectrons per time step; b) at 980 km height, 20:40:24 numerical photoelectrons per time step; and c) at 1380 km height, 0:24:40 numerical photoelectrons per time step. The rates of energy deposit given in HN lead to fluxes of $1.25 \times 10^9, 6.25 \times 10^8$, and 2.5×10^8 photoelectrons cm^{-2} s^{-1}, below 1 keV, at column mass m equal respectively to 10^{-2}, 10^{-3}, and 10^{-4} g cm^{-2}.

Due to strong collisions in dense layers of the solar atmosphere, the saturation state is reached in very short times: $t_S \sim 3 \times 10^{-6}$ s at 675 km height, $t_S \sim 3 \times 10^{-5}$ s at 980 km height, and $t_S \sim 1.5 \times 10^{-4}$ s at 1380 km height. The time step τ used in each of the three levels was 1/3 10^{-2} times the corresponding saturation time. At saturation, the photoelectron densities n_{ph}^S at these three heights are respectively 5 10^2, 2.5 10^3 and 6.5 10^3 cm^{-3}. For comparison, the hydrogen densities at the same heights are respectively 4 10^{14}, 3.14 10^{13} and 2.27 10^{12} cm^{-3}, and the densities of local electrons with a energy higher than 12 eV, able to populate by collisional excitation the upper level of the Hα transition, are accordingly 5 10^2, 2.5 10^3 and 6.5 10^3 cm^{-3}.

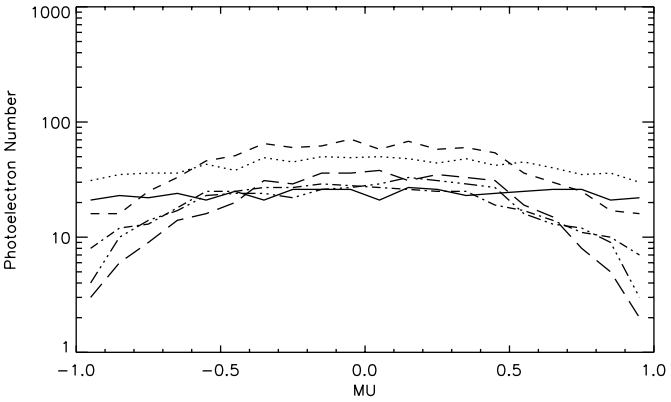

Fig. 1. The photoelectron distribution functions for six electron energy intervals: 0–0.166 keV (*full line*), 0.166–0.333 keV (*dotted line*), 0.333–0.500 keV (*dashed line*), 0.500–0.666 keV (*dash-dot line*), 0.666–0.833 keV (*dash-dot-dot-dot line*), and 0.833–1.000 keV (*long dashed line*) at saturation (t_S = 3.0 × 10^{-6} s), at 675 km height.

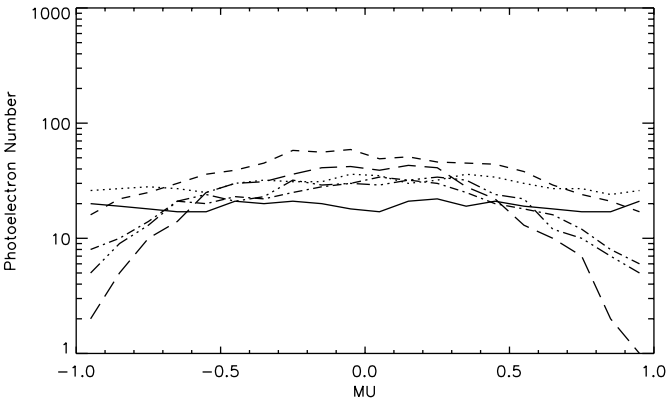

Fig. 2. The photoelectron distribution functions for six electron energy intervals: 0–0.166 keV (*full line*), 0.166–0.333 keV (*dotted line*), 0.333–0.500 keV (*dashed line*), 0.500–0.666 keV (*dash-dot line*), 0.666–0.833 keV (*dash-dot-dot-dot line*) and 0.833–1.000 keV (*long dashed line*) at saturation (t_S = 3.0 × 10^{-5} s), at 980 km height.

3.2. Results

At saturation, the resulting μ, where $\mu = \cos\alpha$, dependence of the distribution functions in various energy bands, is obtained by adding the contribution of all numerical photoelectrons. This dependence is shown, at heights 675, 980 and 1380 km, in Figs. 1–3. The higher the photoelectrons energy, the higher their remaining anisotropy. Photoelectrons in the high energy band 833 eV to 1 keV are left with a significant maximum of their velocity distribution function at 90° from the axis of symetry of the X-ray irradiation. On the other hand, photoelectrons in the lower energy channel 0 to 166 eV are nearly fully isotropised.

To express the anisotropy of the distribution functions $f(E, \alpha)$, the associated anisotropy function

$$B(E) = \frac{3J_2(E) - J_0(E)}{2J_0(E)} \tag{11}$$

was calculated in every photoelectron energy band and at each height.

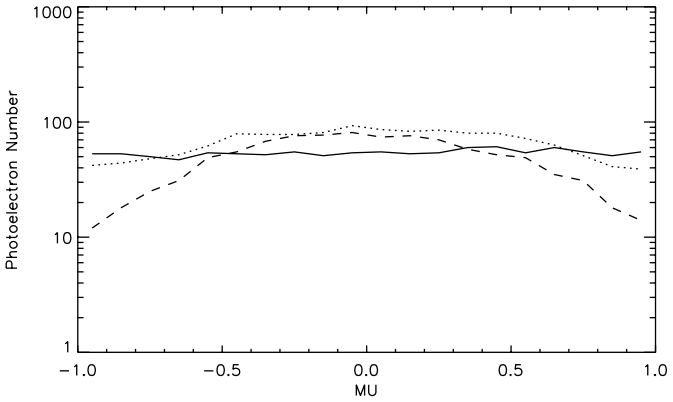

Fig. 3. The photoelectron distribution functions for three electron energy intervals: 0–0.166 keV (*full line*), 0.166–0.333 keV (*dotted line*), and 0.333–0.500 keV (*dashed line*), at saturation (t_S = 1.5 × 10^{-4} s), at 1380 km height.

The values of the functions $B(E)$, for various energy ranges, at the three heights of 675, 980 and 1380 km are summarized in Tables 1–3.

3.3. Polarization generated by photoelectrons alone

The degree of linear polarization, $P(\theta)$, of a line collisionally excited by particles having a velocity distribution function $f(E, \alpha)$ symmetrical around the local solar vertical at a heliocentric angle θ, is given by Eq. 5

For a given photoelectron energy band $E \pm \Delta E$, line radiation is generated with a polarization degree that does not exceed the product of $B(E)$ by the maximum amplitude of the polarization degree $P(90°, E)$ observed at $90°$ of an electron beam. $P(90°, E)$ goes from about 20% near the excitation threshold to about -20% (Kleinpoppen, 1969) at high energy. Low energy photoelectrons being isotropized, the contribution to the line polarization of photoelectrons of energy above 200 eV is dominant. From Tables 1, 2 and 3, it appears that the maximum of polarization of the Hα emission generated by phoelectrons alone does not exceed $\simeq 4\,\%$. This linear polarization is radial.

Since local thermal electrons and radiation field generate unpolarized Hα radiation, the maximum of polarization will be lower than the one generated by photoelectrons alone. We expect the polarization to be reduced in the ratio of the non-thermal to thermal line emission. Therefore, the relative contribution of photoelectrons to the Hα line intensity must be estimated.

4. Net Hα polarization expected from X-ray irradiation

4.1. Phoelectron contribution to the Balmer lines intensities

Photoelectrons contribute to the collisional excitation of the hydrogen Balmer and Lyman lines. Calling dE^H/dt the rate of energy deposited by soft X-ray irradiation of the solar atmosphere, the rates of non-thermal collisional excitation of the hydrogen levels 2 to 4 and of the continuum are respectively (Fang, Hénoux and Gan, 1993):

Table 1. Energy dependence of the function $B(E)$ associated with the photoelectron velocity distribution function at the height of 675 km.

Photoelectron Energy (keV)	B(E)
0–0.166	−0.019
0.166–0.333	−0.064
0.333–0.500	−0.169
0.500–0.666	−0.160
0.666–0.833	−0.192
0.833–1.000	−0.253

Table 2. Energy dependence of the function $B(E)$ associated with the photoelectron velocity distribution function at the height of 980 km.

Photoelectron Energy (keV)	B(E)
0–0.166	−0.009
0.166–0.333	−0.043
0.333–0.500	−0.154
0.500–0.666	−0.176
0.666–0.833	−0.199
0.833–1.000	−0.284

Table 3. Energy dependence of the function $B(E)$ associated with the photoelectron velocity distribution function at the height of 1380 km.

Photoelectron Energy (keV)	B(E)
0–0.166	−0.005
0.166–0.333	−0.112
0.333–0.500	−0.208

$$C_{12}^{ph} \simeq 2.9410^{10} \frac{1}{n_1} \frac{dE^H}{dt} \quad C_{13}^{ph} \simeq 5.3510^{10} \frac{1}{n_1} \frac{dE^H}{dt}$$

$$C_{14}^{ph} \simeq 1.9110^{9} \frac{1}{n_1} \frac{dE^H}{dt} \quad C_{1c}^{ph} \simeq 1.7310^{10} \frac{1}{n_1} \frac{dE^H}{dt}.$$

As in Fang et al. (1993), these non-thermal rates have been included in the equations of statistical equilibrium that relate the populations of the various hydrogen levels and continuum. The statistical and radiative transfer equations, coupled with the hydrostatic equilibrium and particle conservation equations were solved iteratively. A four-level plus continuum atomic model of hydrogen was used.

The Hα and Hβ line profiles were calculated for two empirical models of the solar atmosphere with and without soft X-ray irradiation. These models were the quiet sun solar model C (Vernazza et al., 1981) and the empirical flare model F_1 (Machado et al., 1980). Two values of the rate of X-ray energy deposit at each given depth of the models were used. They differ by one order of magnitude. The lowest one for the quiet sun was taken from HN, who used a 1 to 300 Å X-ray flux of the order of 2 10^{26} erg s^{-1}. The size of the irradiating X-ray source projected on the solar chromosphere was equal to 2 10^{18} cm^2. The associated

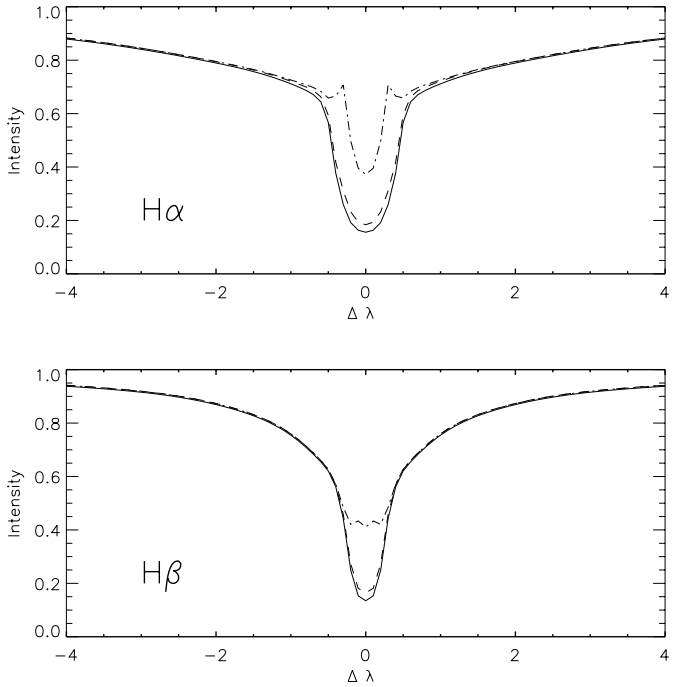

Fig. 4. Hα and Hβ line profiles formed in a quiet sun atmosphere, represented by the empirical model C, without soft X-ray irradiation (*full line*) or irradiated by a solar flare. The soft X-ray flux was equal to (*dashed line*) or ten times higher (*dashed-dotted line*) than the flux used in HN.

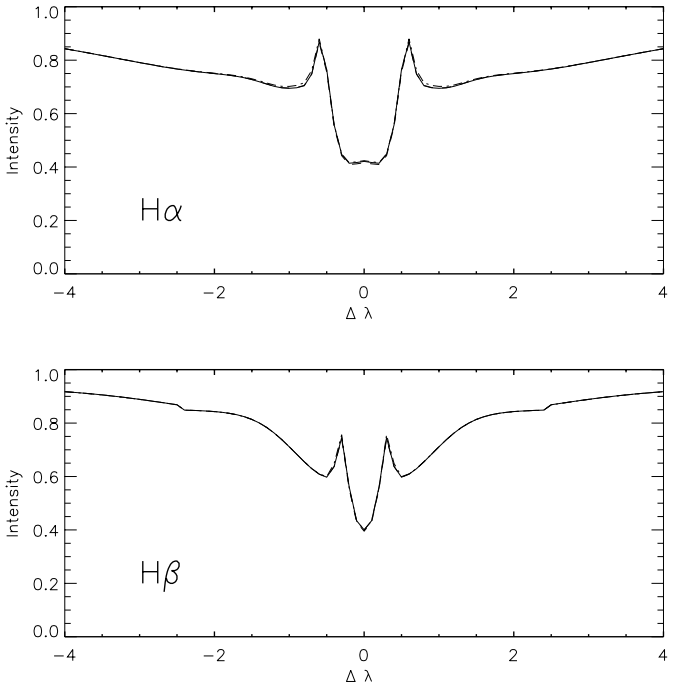

Fig. 5. Hα and Hβ line profiles formed in a flaring solar atmosphere, represented by the empirical flare model F_1, without soft X-ray irradiation (*full line*) or irradiated by the solar flare. The soft X-ray flux was equal to (*dashed line*) or ten times higher (*dashed-dotted line*) than the flux used in HN.

8-12 Å flux corresponds to normal flares of importance 1 (1N flares).

In order to compute the depth dependence of the rate of energy deposit, Hénoux and Nakagawa used the HSRA (Gingerich et al., 1977) empirical model that is close to model C. For computations limited to line intensity profiles, their results could be applied to model F_1 since, for a given X-ray irradiation, the rate of energy deposit in a point of the atmosphere depends only of the difference $m - m_c$ between the column mass m above this point and the coronal mass m_c.

4.2. Resulting line intensities

The resulting line profiles for empirical models C and F_1 are presented in Figs. 4 and 5. For the flare model F_1 the effect of soft X-ray irradiation is negligible. Only for the quiet sun model C are the increases of line intensities significant. The effect takes place near the line centers over $\simeq \pm 0.75$ Å in Hα and over $\pm$ 0.5 Å in Hβ.

4.3. Resulting net linear polarization

The relative non-thermal contribution to the total Hα line emission integrated over $\pm$ 0.75 Å, assuming that the radiation is transmited through a filter with a triangular transmission profile of half width 0.75 Å, is somewhere between 5% (HN soft X-ray flux) and 60% (HN soft X-ray flux $\times$ 10). In the case of Hβ, no observation through a filter have been done yet. Our computations predict that, in the case of observations with a filter with a triangular transmission profile of half width 0.5 Å, the nonthermal contribution to the integrated Hβ line intensity would also be between about 5 and 60%.

The maximum degree of linear polarization expected from soft X-ray irradiation is obtained by multiplying the maximum degree of polarization of the non-thermal emission, generated by the photoelectrons, by the fraction of the total emission they produce. Assumimg that at high energies $P(90^\circ, E)$ is also of the order of -20% in the Hβ line, this leads to a maximum of the polarization degree for both Hα and Hβ lines varying between 0.2 and 2.5%.

5. Discussion and conclusion

The maximum values of the degree of polarization given above have been derived under the assumption that the flaring atmosphere can be described by a quiet sun model. This is not realistic. Soft X-ray heating alone rises the temperature and density of the atmosphere to values close to the ones adopted in the empirical model F_1 (HN). Even using the photoelectrons velocity anisotropy factors computed for model C, this density increase leads to a negligible polarization degree. Since, at a given value of $m - m_c$, the hydrogen number density is higher in model F_1 than in model C, a more exact estimation for model F_1 would have led to a lower anisotropy. With the soft X-ray flux used in

HN and keeping an atmosphere represented by the model C, the expected polarization still does not exceed 0.2%.

Increasing the X-ray flux by a factor ten would certainly lead the atmosphere to conditions close to the ones given in flare models like model F_1. Therefore the highest limit of 2.5% would never be reached. In conclusion, the polarization degree expected from X-ray irradiation cannot exceed 0.2%.

In conclusion, collisional excitation of hydrogen by the photoelectrons generated by X-ray irradiation produces a level of polarization one order of magnitude lower than the observed one. X-ray irradiation cannot explain the Hα line linear polarization observed in solar flares.

Acknowledgements. One autor (M.K.) like to acknowledge the support of the Grant A3003707 of the Academy of Sciences of the Czech Republic. The other (J.C.H.) wishes to thank the French National Center for Scientific Research (CNRS) and the Academy of Sciences of the Czech Republic. Furthermore, both authors thank for their support and kind hospitality both staffs of the Solar Departments at Paris and Ondrejov Observatories. They also thank the Refereee for his valuable comments.

References

Bai T. 1982, ApJ 259, 341
Emslie A.G., 1978, ApJ 224, 241
Evans R., 1955, The Atomic Nucleus. McGraw-Hill Book Company, 695
Fang C., Hénoux J.C., Gan W.Q., 1993, A&A 274, 917
Firstova N., Hénoux J.C., Kazantsev S., Bulatov A., 1997, Solar Phys. 171, 123
Gingerich O., Noyes R.W., Kalkofen W., Cuny Y., 1971, Solar Phys. 18, 347
Heddle D.W.O., 1979, In: Bates D.R., Bederson B. (eds.) Advances in Atomic and Molecular Physics. Academic Press, N.Y., 321
Hénoux J.C, Nakagawa Y., 1977, A&A 57, 105
Hénoux J.C, Rust D., 1980, A&A 91, 322
Hénoux J.C, Vogt E., 1998, Physica Scripta, in press
Hénoux J.C, Heritschi D., Chambe G., et al., 1983, A&A 119, 233
Kleinpoppen H., 1969, In: Bopp F., Kleinpoppe H. (eds.) Physics of the one and two electron atoms. North Holland
Machado M.E., Avrett E.H., Vernazza J.E., Noyes R.W., 1980, ApJ 242, 336
Percival I.C., Seaton M.J., 1959, Phil. Trans. R. Soc. London A 251, 113
Vernazza J.E., Avrett E.H., Loeser R., 1981, ApJS 45, 635
Vogt E., Hénoux J.C., 1996, Solar Phys. 164, 345
Vogt E., Hénoux J.C., 1998, A&A, submitted
Werner A., Schartner K.H., 1996, J. Phys. B: At. Mol. Opt. Phys. 29, 125